

Numerical Investigation of 3D Effects in Hartmann-Sprenger Tubes

Christian Bauer and Oskar J. Haidn

Institute for Flight Propulsion, Technische Universität München, Boltzmannstr. 15, 85748 Garching, Germany

Abstract

CFD simulations of different Hartmann-Sprenger Tube configurations are performed using Ansys Fluent. By utilizing the Thin Wall and Shell Conduction models accurate surface temperatures for axisymmetric 2D simulations are obtained. 3D calculations on a symmetric grid show strong 3D effects in the interaction area between nozzle and cavity, which lead to damping of large-amplitude pressure oscillations without generating realistic heating rates.

Nomenclature

JRM	Jet Regurgitant Mode	ε	Emissivity [-]
JSM	Jet Screech Mode	k	Heat Conductivity [W/(m K)]
CFL	Courant-Friedrichs-Lewy Number	h	Heat Transfer Coefficient [W/m ²]
NPR	Nozzle Pressure Ratio ($p_{\text{Nozzle}} / p_{\text{environment}}$)	a	Speed of sound [m/s]
k_s	Sand Grain Surface Roughness [m]	R	Solid Material Thickness [m]
τ	Characteristic Time [s]	f	Frequency

1 Introduction

The Institute for Flight Propulsion (LFA) at the Technische Universität München (TUM) investigates the properties of the propellants oxygen/methane for use in satellite and upper stage propulsion applications, in order to find replacements for the highly toxic and carcinogenic Hydrazine and its derivatives. In contrast to classical, storable propellants these “green” propellants require a dedicated ignition system. This creates additional challenges for in-space thrusters, where long mission durations and a high number of ignitions are required. Consequently LFA also investigates resonance ignition systems for use in these conditions.

Resonance ignition systems utilize Hartmann-Sprenger-Tubes (HS-tubes) for heat generation, in order to provide either a hot surface or a gas torch as ignition source. These passive devices usually consist of a convergent nozzle, creating an underexpanded free-stream jet impinging on a cavity. A typical configuration can be seen in Fig. 1. By adjusting the nozzle pressure ratio, cavity length and nozzle-cavity distance gas-dynamic resonance can be achieved, leading to strong pressure oscillations and a gradual temperature increase in the resonator cavity.

Since the original discovery [2] [3], Hartmann-Sprenger Tubes have been investigated for more than 50 years. Although an excellent review of the extensive literature is provided by Raman et. Al. [4], a short introduction is also given here.

One of the most conclusive studies has been conducted by Sarohia and Back [1], who identified the main oscillation types occurring inside the resonator cavity.

For low, undercritical Nozzle Pressure Ratios (NPR) vortices shed from the nozzle outlet travel downstream, causing weak pressure waves inside the resonator cavity. Since in this Jet Instability Mode (JIM) neither strong pressure nor thermal effects occur it is not of further interest in the context of this work.

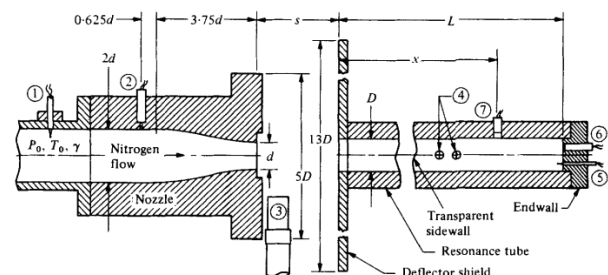


Fig. 1: Classical HS configuration with nozzle (left) and resonator cavity (right) as used by Sarohia and Back. [1]

When the NPR is increased beyond the critical limit, an underexpanded free-stream jet with the typical diamond or barrel-shock structure is generated. Under these conditions, depending on the nozzle-resonator distance (s), a transition to the Jet Regurgitant Mode (JRM) is possible, which can be characterized by two distinct phases. During the inflow phase the free-stream enters the cavity almost unobstructed, creating a series of pressure waves which travel inside the cavity towards the closed end. Given sufficient cavity length, these waves coalesce to a single shockwave, which is reflected at the closed resonator end. When this shock reaches the open cavity end strong expansion waves traveling into the cavity, marking the transition to the outflow phase. During this period the gas leaves the resonator with considerable velocity, displacing the nozzle free-stream upstream. Once the cavity has been emptied, a new inflow cycle starts. It is worth noting that the static pressure inside the cavity can exhibit values exceeding the total pressure of the nozzle and fall below ambient pressure. These strong oscillations occur with approximately the acoustic fundamental frequency of the cavity, but strong non-linear effects can lead to considerable deviations. If the cavity is long enough, a small fraction of the resonance gas remains in the cavity, undergoing repeated compressions and expansions, causing gradual heating due to irreversible effects.

If the NPR or nozzle-resonator distance is changed a sudden switch to Jet Screech Mode (JSM) can occur. In this configuration an almost normal shock between resonator and nozzle can be observed, oscillating in axial direction and emitting compression waves, leading to high-frequency, low-amplitude pressure oscillations in the resonator. Under these conditions Sarohia and Back observed strong heating effect for short resonators and explained these observations by standing waves inside the cavity.

Although the three identified oscillation modes can explain the resulting acoustic spectra, their underlying fluid-mechanical explanation is not completely satisfying, because it cannot explain why in JSM considerable heating only occurs for short resonators, but not for long cavities. Additionally, JRM can also be achieved with Helmholtz-Resonators, exhibiting large-amplitude oscillations between 0.5 and 40 Hz [5] [6] [7], which cannot easily be explained with reflected shock and expansion waves.

Furthermore, a number of modifications to the original HS-configuration exist, which allow maintaining the JRM even in strong subsonic or adapted nozzle flow. These typically aim at reducing the homogeneity or breaking the symmetry of the nozzle flow, for example by introducing a thread across the nozzle axis [3], a needle inside the nozzle [8] [9] or a stem along the resonator [10] [11]. This suggests, that 3D effects may have a considerable influence on the overall flow behaviour.

Preliminary experiments conducted at LFA seem to confirm this. Fig. 2 shows a symmetrical resonator configuration made from thermoplastic PMMA.

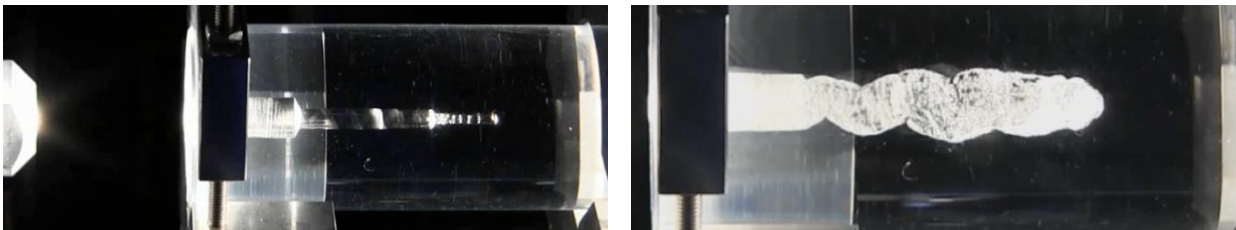


Fig. 2: Resonator cavity made from PMMA in the original configuration (left) and several seconds after start of experiment (right). [12]

During the experiment the gas in the resonator cavity is heated until the melting temperature of PMMA is reached. This leads to severe deformations of the cavity, distorting the originally cylindrical sections into a helix-shaped tunnel. However, whether the observed effect is connected to imperfections in the material or due to instabilities inherent to the flow configuration could not be determined conclusively. Similar features can be identified in earlier 2D axisymmetric CFD simulations, where large vortices inside the resonator cavity can be observed.

Also Kastner and Samimy [13] could observe strong vortices in their experiments, which were not visible in phase-averaged images, requiring a detailed analysis of individual pictures. This is also confirmed by Gregory und Sullivan [14].

Although all these observations seem to suggest that 3D effects may have considerable influence on the overall flow field, all CFD simulations available are performed in 2D calculation domains [9] [15] [16] [17] [18] [19]. The current investigation therefore aims at determining, whether new insights into the mechanisms driving the flow oscillations can be obtained from 3D CFD simulations.

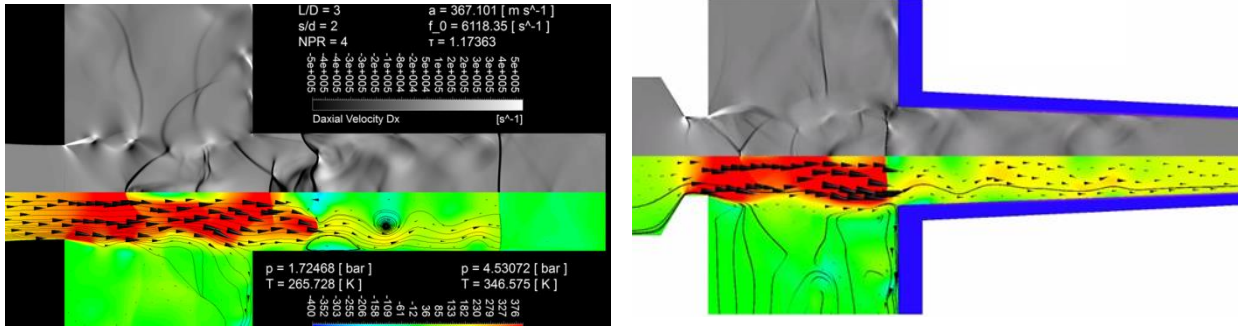


Fig. 3: 2D-axisymmetric CFD simulations of cylindrical and conical cavity, showing large vortex structures during the inflow phase of JRM [20] [12].

2 Numerical Setup

For the present study the commercial CFD solver Ansys Fluent, version 16.0, is used. In earlier investigations it was shown that the density based, explicit formulation of this code can accurately reproduce the shocks occurring in HS-tubes, as well as the resulting acoustic spectrum [20] [12]. However, due to the stability limit of $CFL < 1$ the use of explicit schemes is very restrictive and computationally expensive, requiring meshes highly adapted to the local flow velocities in order to maximize the global timestep size. In the current resonator configuration this limits the timestep size to approximately $2e-10$ s, allowing only for detailed investigations of individual oscillation cycles. However, since a correct prediction of the overall heating performance of the HS-tube is desired for future design optimizations, the pressure based, implicit formulation of the solver is presented in the context of this work. This allows covering larger timeframes at the potential expense of accuracy around strong shocks, requiring experimental data for validation of the resulting simulation results.

Since no new models or major solver modifications are implemented, an extensive discussion of solver theory is omitted. Only the models particular for the current case are discussed in more detail.

2.1 Boundary Conditions and Material Properties

The setup of the present numerical study is based on experiments conducted at LFA, which serve as data base for the validation of the simulations. The experiment, depicted in Fig. 4, consists mainly of the gas feed system, a convergent nozzle mounted on an actuator, and the stainless steel resonator enclosed by an insulation chamber. Nozzle pressure ratio (NPR) and nozzle-resonator-distance (s) can be varied. Pressurized air is used as resonance gas, and its inlet conditions are measured by thermocouples and pressure transducers. Resonator temperatures at the closed end and at the sidewall are measured by additional thermocouples. Farfield acoustic data is sampled at 102.4 kHz by a condenser microphone. Shadowgraph optics capture the area between nozzle outlet and resonator inlet.

By comparing thermocouple data to pyrometer measurements the emissivity factor is estimated to $\varepsilon \approx 0.6$, but has also been observed to change noticeably during individual test runs, due to tarnishing of the resonator surface. A more detailed description of the experiment, as well as an extensive discussion of the measurements, is available in [21].

The resonance medium is modelled as ideal gas, with temperature-dependant values for c_p , k and ν fitted to 0.5 MPa from NIST data [22]. The solid resonator material is not modelled explicitly, but is accounted for by the specified internal and external boundary conditions.

In the 2D case, the Thin Wall model is utilized, solving the steady-state heat conduction equations between inner and outer wall, accounting for radiative and convective heat transfer to the surrounding medium, but neglecting axial heat

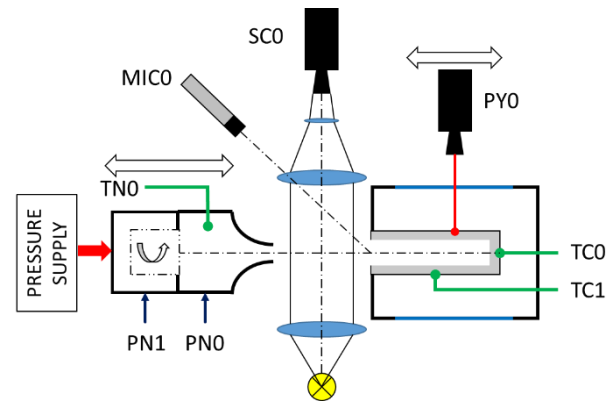


Fig. 4: Experimental setup comprising axially adjustable nozzle with optional swirl generator, test chamber with exchangeable resonators, shadowgraphy optics, microphone and axially movable pyrometer. [21]

transfer. Since axial energy transfer is expected to be considerable, the temperatures occurring in the 2D simulations is only used for a relative comparison. For the 3D simulations the shell conduction model is enabled, which also takes axial heat transport and transient effects into account. However, since flow phenomena and conductive heat transport in the solid occur on different timescales, an adaptation of material properties is implemented.

The timescales of the flow can be characterized by the frequency of the largest oscillations, which can be approximated by the quarter wavelength formula (1):

$$\tau_{osc} = f^{-1} = \left(\frac{a}{4L}\right)^{-1} \quad (1)$$

Due to nonlinear effects noticeable deviations from this ideal value can be observed in experiments, but for the sake of determining the characteristic timescale the agreement is sufficient, leading to $\tau_{osc} \approx 1$ ms.

Characteristic timescales for the heat conduction problem within the resonator solid material are obtained from eq. (2) [23],

$$\tau_{cond} = \frac{R^2 \rho_s c_{p,s}}{k} \quad (2)$$

resulting in $\tau_{cond} \approx 0.4$ s for the sidewall and $\tau_{cond} \approx 30$ s for the closed resonator end, which agrees with experience gained from experiments. This timescale is artificially reduced to $\tau_{cond, bottom} = 5\tau_{osc}$ by adapting the solid's heat capacity to 7.556 kg/m^3 .

For the outer walls the convective heat transfer coefficient is determined from correlations assuming free convection around a horizontal cylinder [24], while the emissivity is obtained from experiments. The heat transfer from the resonance gas to the resonator walls is determined by the code directly, without specifying a dedicated transfer coefficient, relying on heat conduction in the outermost fluid layer. Due to limitations of the Shell Conduction model the walls of the stem are modelled as adiabatic. For both resonator and stem walls a sand grain roughness of $6.3 \mu\text{m}$ is specified, while the nozzle walls are considered smooth. At the outlet a total pressure of 0.1 MPa is specified.

Radial profiles for flow and turbulence properties at the inlet are obtained from precursor simulations of the upstream flow area not presented in the context of this work.

An overview of the calculation domain and the specified boundary conditions is given in Fig. 5, while the geometric parameters are summarized in Table 1.

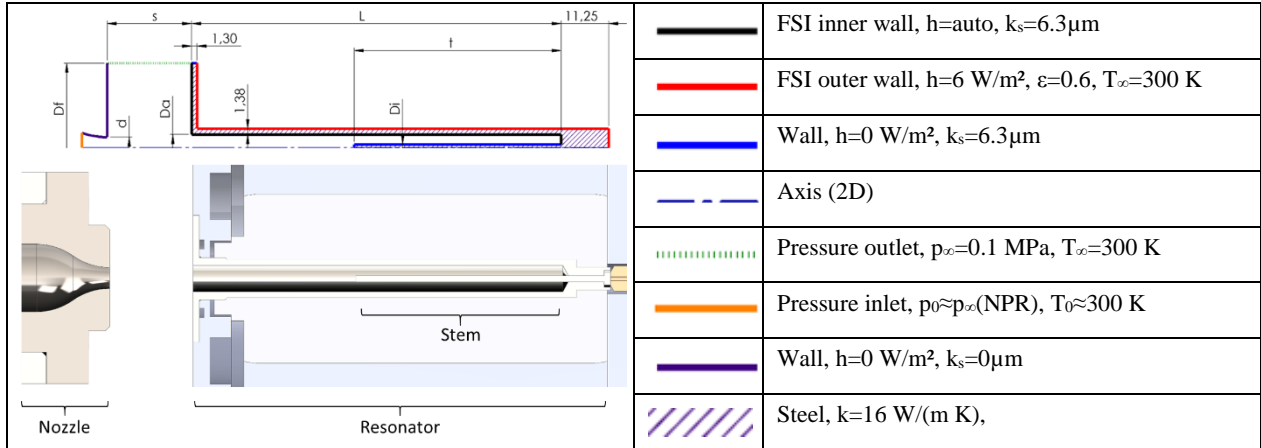


Fig. 5: Boundary conditions of the calculation domain for all simulations. Note that inlet conditions are specified as radial profiles of p_0 , T_0 , k and ω obtained from precursor simulations not presented here.

Table 1. Characteristic dimensions of nozzle, resonator and stem

d	Da/d	Di/d	t/L	L/D
5 mm	1.25	0.3	0.56	14

2.2 Numerical Schemes, Models and Discretization

The investigated flows, dominated by strong, instationary shockwaves, create a challenging environment for pressure based solvers which requires a careful selection of the applied discretizations and schemes. A short summary of the applied settings is given here.

The coupled, pressure based solver stores scalar values at the cell centre. These are extrapolated to cell-surfaces by applying the QUICK upwind scheme for all variables except pressure, for which a second order upwind scheme is used. In conjunction with node based Green-Gauss gradient evaluation this allowed for good shock resolution while avoiding “aftershocks” following the incident shockwave observable for other schemes. Bounded Second Order Implicit discretization is used for time integration. Cell-to-Cell values of the reconstructed gradients are clipped by the multidimensional limiter, since the differential limiter caused residual stalling under some circumstances.

Turbulence is modelled by the $k-\omega$ SST model, accounting for compressibility effects and viscous heating. Excess turbulence production is limited by a clip factor of 10.

2.3 Computational Mesh

The hex mesh depicted in Fig. 6 serves as the basis for refinement studies. Since fluid-solid heat transfer is of interest, a boundary layer resolution of $y^+ \approx 1$ is desired. However, since the fluid periodically reverses direction at high velocities this value cannot be maintained for all time steps, but the introduced inaccuracy is considered small.

Since the flow under investigation is inherently unstable, a comparably inexpensive steady-state solution for mesh convergence studies does not exist. However, by using highly dissipative numerical schemes, very low URFs and a very coarse mesh, an artificial stationary solution can be obtained. The mesh is then repeatedly refined in all spatial directions. For a refinement factor of 1.75, oscillations in the steady-state solution occur and the solution can no longer be converged. This suggests, that beyond this refinement the most relevant physical processes can be reproduced even with highly dissipative schemes, and that good accuracy can be obtained for higher-order simulations.

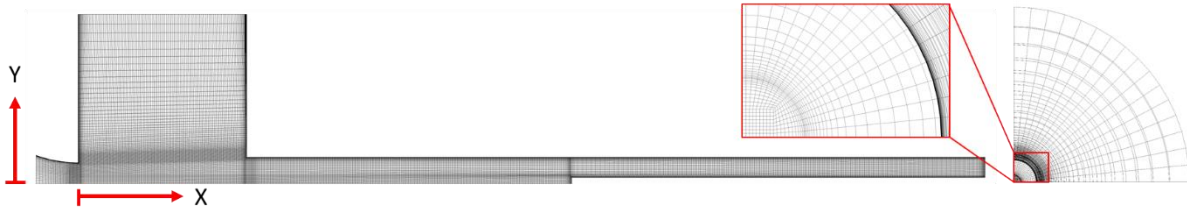


Fig. 6: Hex mesh topology and sizing for a refinement factor of 1.0, resulting in $\approx 30k$ elements for the 2D case and $\approx 2M$ elements for 3D. Note that only a quarter of the circumferential direction is shown.

In order to confirm this conclusion a number of transient 2D simulations is performed on meshes with and without the axial stem. This allows testing the robustness of the mesh topology and setup by validating the obtained results against additional experimental data only available for no-stem configurations.

Due to the strong instability of the flow exact agreement between the same timesteps of different meshes cannot be obtained, almost independently of mesh resolution. During the outflow phase of the first flow cycle highly dynamic flow patterns occur, which are locally sensitive to even slight parameter changes. This effect is accumulated with each oscillation cycle, increasing successively the deviations between individual simulations.

However, Fig. 7 (left) shows the static temperature averaged over the total simulation time of 4 ms along the rotational axis. Good agreement of thermal effects between all meshes can be observed. The reason for this lies in the good reproduction of the pressure oscillations, depicted in Fig. 7 (right), which are to be considered the main heating mechanism.

It is worth noting, that the area of the largest temperature increase predicted by the simulation agrees well with tempering colours observable on the resonator surface after experiments. Since the steep increase around $x=0.08$ m does not correlate to pressure data, this highlights the area where mass exchange between resonator fluid and environment is considerably reduced.

Since neither of the investigated meshes exerts noticeable influence on the integral pressure and temperature data, a medium refinement factor of 1.75 is used for all further studies, which results in 80k – 100k elements, depending on s/d.

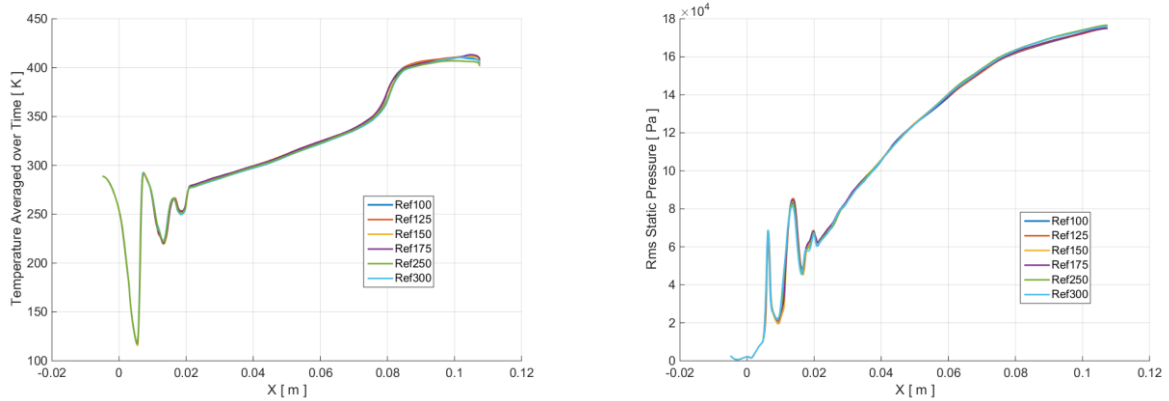


Fig. 7: Comparison of time-averaged static temperature and RMS of static pressure at the rotation axis for different mesh resolutions after a simulation time of 4 ms.

2.4 Validation of 2D Cases

For validation purposes the selected mesh is also used for a parametric study correlating the resonator endwall temperature increase to various NPRs for an s/d of 4. The total simulation time is limited to ≈ 10 ms, therefore only comparative conclusions can be drawn. Fig. 8 compares experimental data obtained by Sarohia/Back and LFA to the simulated resonator configuration without stem.

The experiments conducted at LFA show a sudden drop in end-wall temperature between $NPR=3.8$ and 4.5 , which is not reported by Sarohia and Back and is also not reproduced by the simulation. No satisfactory explanation for this low-temperature region could yet be found. The strong increase in temperature between $NPR=3.5$ and 4.2 , marking the transition from JSM to JRM, is well reproduced by numerical results. Although good agreement between numerics and experiment is found for $NPR > 4.2$ this should be considered coincidental, since the simulation time is too short to achieve a thermal quasi-steady state. Transient temperature traces show that the initial pressure-hammer effect, created from the starting conditions, leads to elevated temperatures during the initial inflow phase, which are consequently relaxed during successive flow cycles.

A comparison of the acoustic spectra between simulation and experiment shows good agreement of the low frequency oscillations. Note that the amplitudes of the spectra in Fig. 9 are rescaled for ease of comparison, since experimental data are obtained approx. 1 m from the resonator inlet, while the simulation is evaluated in the vicinity of the resonator.

A further parametric study for a resonator configuration with a non-dimensional stem length of $t/L=0.56$ and a fixed NPR of 4.5 is conducted and compared to the LFA experiments. Resonator setups with s/d ratios of 3.0, 3.8 and 5.5 are simulated for a total time of 100 ms each. Transient pressures and temperatures show that thermal equilibrium and quasi steady state is reached after ≈ 50 ms for setups with high heating rates. The systems exhibiting less heating and less violent oscillations reach equilibrium after ≈ 20 ms. Although Niwa et. Al. used oxygen as resonance gas and

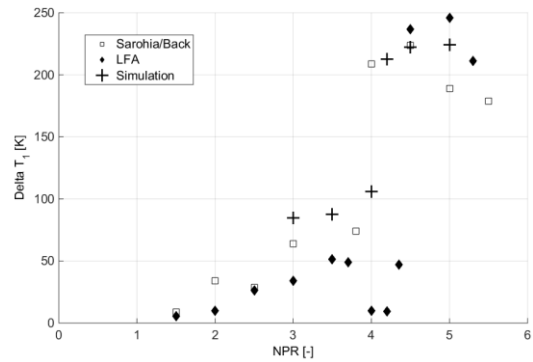


Fig. 8: Comparison of endwall temperatures for $s/d=4$ between simulation data and experiments conducted by Sarohia/Back and at LFA [21] [1] over various NPRs.

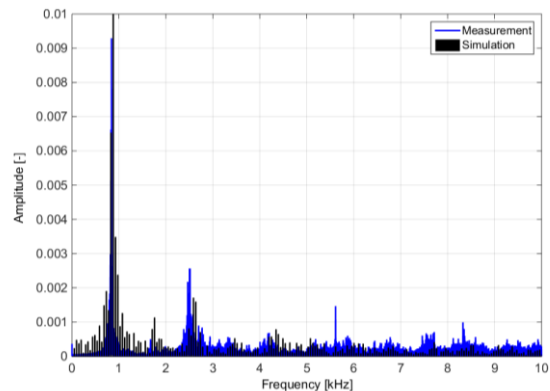


Fig. 9: Comparison of the acoustic response spectrum of experiment and simulation for resonator without stem at $s/d=4$ and $NPR=4.5$.

a cavity of unspecified dimensions they report in their tests [25] gas-dynamic ignition in less than 50 ms, which shows that the simulated heating rates are also feasible in reality.

For the configuration, in which the resonator flow exhibits JRM behaviour, the simulation overpredicts the final end-wall temperature by about 50 K, as can be seen in Fig. 10. This may be attributed to the limitations imposed by the Thin Wall model, which does not account for axial heat conduction in the resonator material. However, the heating rates for $s/d=3.0$ and 5.5 are underpredicted by around 30 K. The reason for this behaviour can currently not be explained satisfactory, but may be related to higher-order oscillations which are not reproduced accurately.

For the current investigation the occurring deviations are considered acceptable, since the general characteristics of the experiments can be reproduced qualitatively. The mesh is therefore extended in circumferential direction for the following 3D simulations. Particular care is taken to avoid asymmetries in the mesh by mirroring and copying an initial 90° wedge, resulting in a total of $\approx 9M$ elements.

3 Results of 3D Simulation

For the 3D simulations the resonator configuration with stem and $s/d=3.8$ at $NPR=4.5$, which during experiments exhibited the highest heating rates, is selected for further study. Despite the good agreement of the 2D simulations presented in section 2.4 with experimental data, no comparable heating rates can be observed in the 3D case. Fig. 11 compares the static pressure signal inside the resonator cavity for both simulation setups and shows, that the 2D simulations reproduce the typical JRM behaviour with strong pressure oscillations at approximately cavity quarter wavelength frequency. For the 3D case however, the initial pressure wave is dampened almost completely after the 2nd flow cycle with only high frequency screech occurring afterwards.

Fig. 14 visualizes the flow by density gradients during different in- and outflow phases for both simulations. Although the flow is highly symmetric during the first 0.2 ms small distortions occur in the wake of the first barrel shock. These distortions lead to slightly unsymmetrical inflow during the first oscillation cycle and are convected downstream into the resonator. At the closed resonator end they are reflected and lead to asymmetric outflow, further increasing the inhomogenities during the next inflow phase, amplifying this effect with each oscillation cycle. After 6 ms the overall flowfield is distorted to such a degree, that the nozzle flow is no longer axially aligned to the resonator.

The most severe difference between 2D and 3D simulations can be seen in Fig. 14 for 0.8 ms. In the 2D case the nozzle jet is pushed back by the resonator outflow up to the first barrel shock, while the outflow is severely inhibited for the 3D simulation. It is worth noting that this already allows evaluating, whether resonance occurs in the system, even before the first flow cycle is completed, which may be useful for further investigations.

Iwamoto investigated the different phases of resonator flow and deduced from pressure and schlieren data, that the outflow is critical for achieving resonance and that a low-pressure region around the resonator inlet is required during this phase [26]. Fig. 12 shows, that this condition is met for both simulations, but that the low-pressure region for the 3D case is highly distorted. For reference the mirror planes, with which the original 90° wedge mesh was extended to 360° is included, which shows that the pressure fluctuations do not coincide with any of these directions.

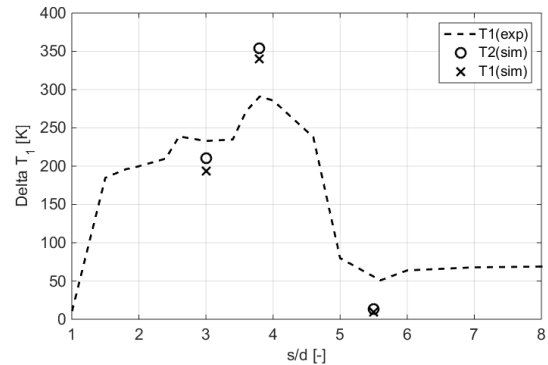


Fig. 10: Comparison of end-wall (T2) and side-wall temperatures (T1) between experiment and simulation for different s/d values.

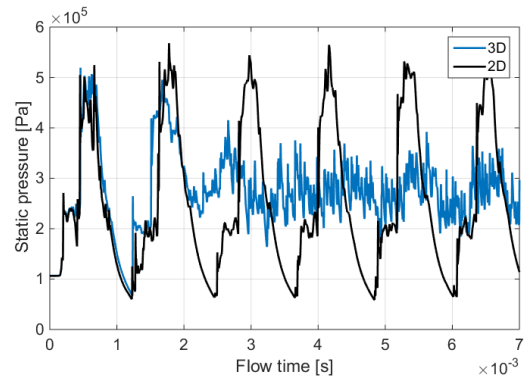


Fig. 11: Development of static pressure inside resonator for 2D and 3D simulations over 7 ms.

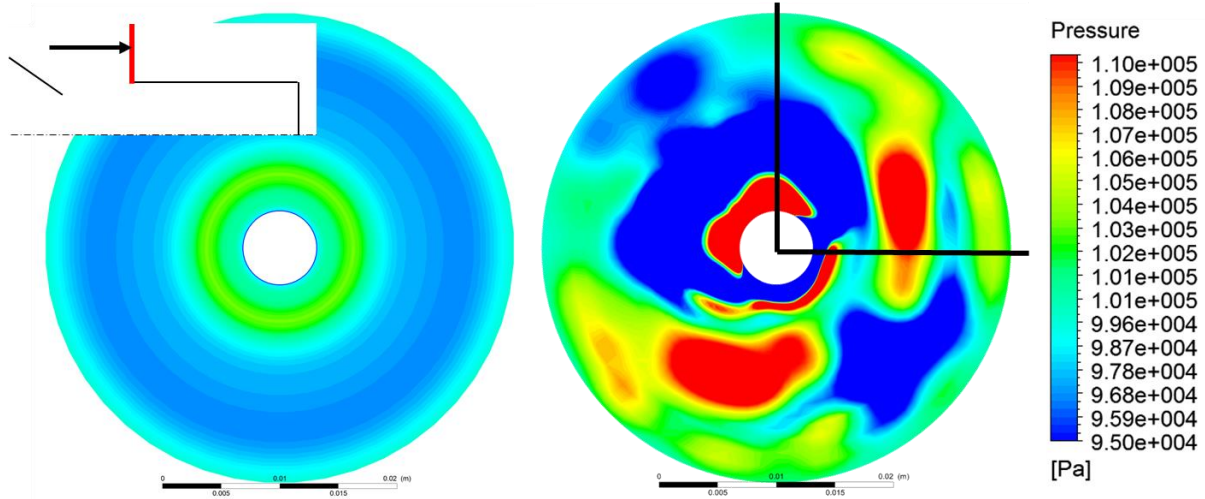


Fig. 12: Pressure distribution at planar wall around resonator inlet for 2D (left) and 3D (right) simulation at 0.8 ms. The symmetry axes of the 3D mesh are drawn black, which shows that the strong pressure variations do not correlate with mesh features.

The second condition proposed by Iwamoto for obtaining stable oscillatory flow is the existence of a positive pressure gradient in front of the resonator. Fig. 13 shows the axial pressure distribution for both cases and shows, that such a region exists in the form of the first barrel shock generated by the nozzle. However, a comparison with Fig. 14 suggests, that for the 3D case the outflow velocities are too slow to reach this area and therefore this condition is not met for the 3D simulations.

However, the presented preliminary evaluations only show the effects of fundamental differences between 2D and 3D simulations, the cause for the decidedly different flowfield has yet to be found. Further investigations are ongoing and the 2D models are to be tested against additional resonator configurations.

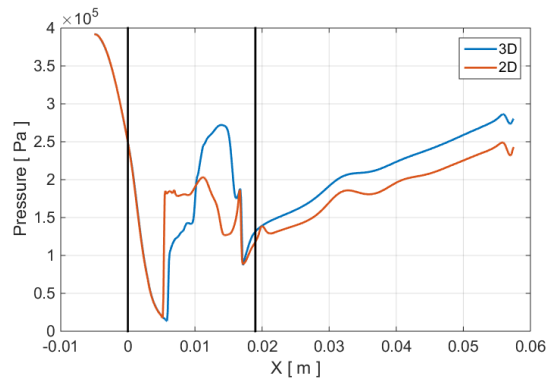


Fig. 13: Axial pressure distribution for both simulations at 0.8 ms, which marks the main outflow phase of the first cycle. The vertical lines mark the position of the nozzle outlet (left) and resonator inlet (right).

4 Conclusions

Numerical simulations of the flow in Hartmann-Sprenger Tubes are conducted and compared to experimental results. The pressure based version of the Ansys Fluent solver is used throughout the studies. Fluid-Solid-Interaction is included by implicitly modelling the solid walls using the Thin Wall and the Shell Conduction Model, accounting for heat conduction in the solid and convective and radiative heat losses to the environment, representing the experimental conditions more closely than adiabatic calculations. 2D axisymmetric simulations of a convergent nozzle operated with air at various nozzle pressure ratios impinging on a simple cylindrical cavity show good qualitative agreement with experimental results. For a fixed nozzle distance ratio of $s/d=4.0$ the switch from JSM to JRM at $NPR=4$ is reproduced and the low-frequency spectra agree. A HS-Tube configuration employing a coaxial stem fixed at the resonator bottom is simulated for a total flowtime of 100 ms, while neglecting capacitive effects in the solid material. Evaluations show, that a thermal quasi-stationary condition is reached after less than 50 ms. Quantitative agreement of measured and simulated temperatures is satisfactory.

The identical boundary condition setup for a 3D simulation shows decidedly different results. Due to strong, dynamic 3D effects the necessary conditions for maintaining stable flow oscillations are no longer met and JRM oscillations are dampened after ≈ 3 flow cycles without attaining considerable heating rates. Investigations for identifying the root cause for this behaviour are ongoing.

5 Acknowledgments

The presented work has been kindly supported by Munich Aerospace e. V. The authors also gratefully acknowledge the Gauss Centre for Supercomputing e.V. (www.gauss-centre.eu) for funding this project by providing computing time on the GCS Supercomputer SuperMUC at Leibniz Supercomputing Centre (LRZ, www.lrz.de).

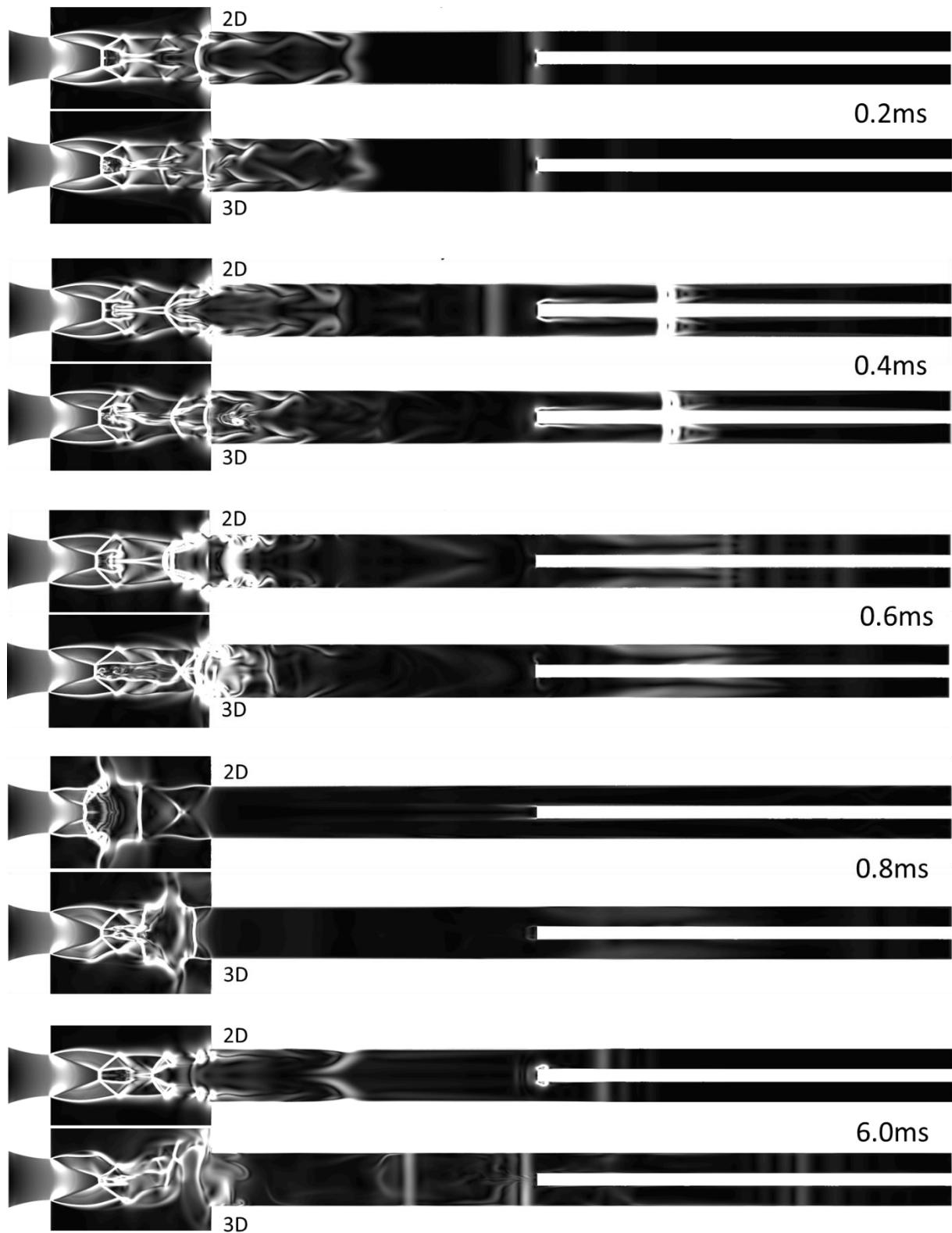


Fig. 14: Flow visualized by density gradient for 2D and 3D simulation for various timesteps. While the flow inside the resonator cavity is highly symmetric the domain between nozzle and resonator inlet exhibits strong asymmetries in the 3D calculations.

6 References

- [1] V. Sarohia und L. Back, „Experimental Investigation of Flow and Heating in a Resonance Tube,“ *J. Fluid Mech.*, Nr. 94, 1979.
- [2] J. Hartmann, „On a New Method for the Generation of Sound Waves,“ *Physics Review*, no. 20, 1922.
- [3] H. Sprenger, „Über thermische Effekte in Resonanzrohren,“ *Mitteilungen aus dem Institut für Aerodynamik an der ETH Zürich*, 1954.
- [4] G. Raman and K. Srinivasan, „The powered resonance tube: From Hartmann's discovery to current active flow control applications,“ *Progress in Aerospace Sciences*, no. 45, 2009.
- [5] T. Smith und A. Powell, „Experiments Concerning the Hartmann Whistle,“ University of California, Los Angeles, 1964.
- [6] J. Hartmann und B. Trolle, „New Investigation on the Air Jet Generator for Acoustic Waves,“ 1926.
- [7] W. Jungowski und G. Grabitz, „Self-sustained oscillation of a jet impinging upon a Helmholtz resonator,“ *Journal of Fluid Mechanics*, vol. 179, 1987.
- [8] E. Brocher, C. Maresca und M. Bournay, „Fluid Dynamics of the Resonance Tube,“ *Journal of Fluid Mechanics*, Nr. 43, 1970.
- [9] G. Xia, D. Li und C. Merkle, „Effects of a Needle on Shrouded Hartmann-Sprenger Tube Flow,“ *AIAA Journal*, vol. 45, no. 5, 2007.
- [10] J. Litsios, „Industrial Application of Gas-Jet Sonic Generators,“ *IEEE Transactions on Ultrasonic Engineering*, 1963.
- [11] Y. Borisov, „Acoustic gas-jet generators of the Hartmann type,“ *Sources of high-intensity ultrasound*, Nr. 1, 1969.
- [12] C. Bauer und O. Haidn, „Numerical and Experimental Investigations on Resonance Ignition,“ in *Space Propulsion Conference*, Köln, 2014.
- [13] J. Kastner und M. Samimy, „Development and Characterization of Hartmann Tube Fluidic Actuators for High-Speed Flow Control,“ *AIAA Journal*, vol. 40, no. 10, 2002.
- [14] J. Gregory und J. Sullivan, „Characterization of Hartmann Tube Flow With Porous Pressure-Sensitive Paint,“ in *33rd AIAA Fluid Dynamics Conference and Exhibit*, Orlando, FL, 2003.
- [15] O. Inoue, S. Imuta, B. Milton und K. Takayama, „Computational study of shock wave focusing in a log-spiral duct,“ *Shock Waves*, vol. 5, 1995.
- [16] B. Li, G. Hu und Z. Zhou, „Numerical simulation of flow in Hartmann resonance tube and flow in ultrasonic gas atomizer,“ *Applied Mathematics and Mechanics (English Edition)*, vol. 28, 2007.
- [17] S. Murugappan und E. Gutmark, „Parametric study of the Hartmann-Sprenger tube,“ *Experiments in Fluids*, vol. 38, 2005.
- [18] A. Cain, E. Kerschen, J. Tassy und G. Raman, „Simulation of Powered Resonance Tubes: Helmholtz Resonator Geometries,“ in *2nd AIAA Flow Control Conference*, Portland, Oregon, 2004.
- [19] A. Hamed, K. Das und D. Basu, „Numerical Simulation and Parametric Study of Hartmann-Sprenger Tube Based Powered Device,“ in *41st Aerospace Scienced Meeting and Exhibit*, Reno, Nevada, 2003.
- [20] C. Bauer und O. Haidn, „Numerical and Experimental Investigations on Gas-Dynamic Resonance Ignition,“ in *Ansys Conference and CADFEM User's Meeting*, Mannheim, 2013.
- [21] C. Bauer, M. Hauser und O. Haidn, „Investigation of Stabilization Effects in Hartmann-Sprenger-Tubes,“ in *30th International Symposium on Space Technology and Science (ISTS)*, Kobe, 2015.
- [22] E. Lemmon, M. L. Huber und M. O. McLinden, „NIST Standard Reference Database 23, Version 9.0,“ 2010.
- [23] E. Marin, „Characteristic dimensions for heat transfer,“ *Latin-American Journal of Physics Education*, 2010.
- [24] Incropera, DeWitt, Bergmann und Lavine, *Fundamentals of Heat Transfer*, 6th ed.
- [25] M. Niwa, K. Kessaev, A. Santana Jr. und Valle, „Development of a Resonance Igniter for GO₂/Kerosene Ignition,“ in *AIAA 2000-3302*, 2000.
- [26] J. Iwamoto, „Necessary Conditions for Starting and Maintaining a Stable Oscillatory Flow in a Hartmann-Sprenger Tube,“ in *Flow Visualization*, vol. 4, 1986, p. 507.